crystals

MDPI

Article

Ternary Aluminides of a New Homologous Series—$CePt_2Al_2$ and $CePt_3Al_3$: Crystal Structures and Thermal Properties

Elena Murashova *, Yuliya Morozova, Sergey Dunaev, Zhanafiya Kurenbaeva and Anna Tursina

Department of Chemistry, Moscow State University, 119991 Moscow, Russia; yu.s.morozova@mail.ru (Y.M.); dunaev@general.chem.msu.ru (S.D.); kurenbaeva@mail.ru (Z.K.); tursina@general.chem.msu.ru (A.T.)

* Correspondence: murashova@general.chem.msu.ru

Received: 13 March 2020; Accepted: 22 May 2020; Published: 1 June 2020

Abstract: In the process of studying the Ce–Pt–Al system, we identified $CePt_2Al_2$ and $CePt_3Al_3$, two new ternary intermetallic compounds. $CePt_2Al_2$ aluminide undergoes a structural phase transition from a low-temperature orthorhombic modification (of its own structure type, *Cmme*, a = 5.84138(2) Å, b = 6.39099(3) Å, c = 10.11611(5) Å) to a high-temperature tetragonal modification ($CaBe_2Ge_2$ type, *P*4/*nmm*, a = 4.3637(9) Å, c = 10.0925(14) Å) at 280(1) °C. $CePt_3Al_3$ crystallizes with a new type of structure (*Cmme*, a = 6.36548(6) Å, b = 5.78301(6) Å, c = 13.36245(19) Å) built of structural units of low-temperature orthorhombic $CePt_2Al_2$-type and CsCl-type.

Keywords: intermetallic compounds; synthesis; crystal structure; phase transition

1. Introduction

The RET_2X_2 family (RE, rare earth element, actinoid, element of the 2nd group; T, transition metal; X, s- or p-block element) continues to attract attention from scientists due to their different physical properties related to strong electronic correlations such as heavy fermion states, superconductivity, valence fluctuations, unusual magnetic, and non-Fermi liquid behavior [1–7]. Most RET_2X_2 compounds crystallize in two structure types: $CaBe_2Ge_2$ (*P*4/*nmm*, a = 4.02(2) Å, c = 9.92(2) Å) [8] and $ThCr_2Si_2$ (*I*4/*mmm*, a = 4.043(1) Å, c = 10.577(2) Å) [9]. Both are ternary $BaAl_4$-type derivatives [10]. In the $BaAl_4$ structure type, Al atoms reside in two crystallographically different Wyckoff sites: 4*d* (0,1/2,1/4) and 4*e* (0,0,*z*). Those occupying 4*d* sites form two-dimensional square nets that are alternately capped above and below the plane by the atoms in 4*e* sites. Between the corrugated layers perpendicular to [001], Ba atoms are located.

The structure of $ThCr_2Si_2$ is an ordered version of $BaAl_4$ with more than 1700 ternary intermetallics being known as isotypic. In the $ThCr_2Si_2$ type, 4*d* positions are filled by Cr, whereas those in 4*e* are occupied by Si atoms. Thus, the Cr atoms comprise the basal two-dimensional slab of square nets with Si atoms capping the nets in a "checkerboard" pattern. The corrugated $[Cr_2Si_2]$ layers are inverted with respect to each other and are separated by Th atoms. The structure remains *I*-centered like the $BaAl_4$ prototype.

In the structure of $CaBe_2Ge_2$, which is not as rich in ternary intermetallics, filling the square nets of the basal slab and the capping layers occurs in an alternating manner. If the basal slab in the first layer is formed by Be atoms with Ge capping the square nets, in the next layer, Ge atoms build the basal slab that is capped by Be atoms. Due to this architecture of staggered $[Be_2Ge_2]$ layers, $CaBe_2Ge_2$ has a primitive unit cell. Remarkably, $CaBe_2Ge_2$ type intermetallics are more likely to demonstrate superconductivity at high temperatures [11].

Intermetallics with platinum—$REPt_2X_2$ most commonly crystallize in the $CaBe_2Ge_2$ type. Silicides $REPt_2Si_2$ (RE = Y, La–Nd, Sm, Gd–Lu, U, Th) crystallize in a $CaBe_2Ge_2$ type and do not undergo

phase transition [12], although it has been previously reported [13,14] that they belong to the $ThCr_2Si_2$ type with statistical filling of 4*d* and 4*e* positions with Pt and Si atoms in space group *I*4/*mmm*. Platinum germanides $REPt_2Ge_2$ (RE = Ca, Y, La−Dy) demonstrate a monoclinic variant ($P2_1$) of tetragonal $CaBe_2Ge_2$ structure with parameters for $LaPt_2Ge_2$ a = 4.401 Å, b = 4.421 Å, c = 9.851 Å, and β = 90.50° [15]. Reinvestigation of the structure showed a doubling of one of the parameters: a = 9.953 Å, b = 4.439 Å, c = 8.879 Å, β = 90.62°, and $P2_1/c$. The monoclinic cell undergoes a phase transition to a tetragonal type $CaBe_2Ge_2$ when the temperature is increased [16]. No phase transitions were observed in the $CePt_2Sn_2$ stannide, which belongs to the $CaBe_2Ge_2$ type [17].

Several pnictides with a $REPt_2X_2$ composition (X = P, As, Sb) with RE = Eu, Ca, Sr, Ba [18,19] adopt a $CaBe_2Ge_2$ type. $REPt_2P_2$ compounds where RE = Ca, Eu crystallize in a new structure type, a variation of the $CaBe_2Ge_2$ structure with a doubled c parameter and space group *I*4/*mmm*. The structures of $SrPt_2Sb_2$, $BaPt_2As_2$, and $EuPt_2Sb_2$ pnictides belong to the $CaBe_2Ge_2$ type, while the $SrPt_2As_2$ and $EuPt_2As_2$ arsenides present an orthorhombic distortion (*Pmmn*) of its tetragonal cell. Both compounds exhibit polymorphism: the orthorhombic modification of $EuPt_2As_2$ transforms to a tetragonal type $CaBe_2Ge_2$ with increasing temperatures, while $SrPt_2As_2$ undergoes phase transition to a monoclinic ($P2_1/c$) cell when pressure is increased.

About half of the 30 known aluminides RET_2Al_2 demonstrate a structure similar to $CaBe_2Ge_2$ including T = Au, RE = La−Nd, Sm, Eu, Gd−Dy, Th, U, and Sr [20] as well as T = Pd, RE = La, Ce [21]. The two latter compounds exhibit structural instability at low temperatures [22].

Recently, a homologous series structurally related to the title compounds was described [23]. Cerium palladium aluminides with the general formula $CePd_nAl_n$ (n = 2–4) are built from $CaBe_2Ge_2$ and CsCl type structural fragments and crystallize in a tetragonal *P*4/*nmm* space group.

During our ongoing investigation of the Ce–Pt–Al phase diagram, two novel ternary aluminides were observed. Cerium platinum aluminum intermetallics $CePt_2Al_2$ and $CePt_3Al_3$ present a new homologous series $CePt_nAl_n$ with n = 2, 3, derived from the orthorhombic $CePt_2Al_2$ and distorted CsCl type. Preliminary data on the crystal structures of the orthorhombic $CePt_2Al_2$ and $CePt_3Al_3$ have been presented at conferences [24,25]. Herein, we report on two structural modifications of $CePt_2Al_2$, tetragonal and orthorhombic, the structural phase transition between them as well as the crystal structure of $CePt_3Al_3$ and peculiarities of the homologous series $CePt_nAl_n$ (n = 2, 3).

2. Materials and Methods

2.1. Synthesis

The synthesis of new compounds was performed using metallic cerium (99.98%), platinum (99.99%), and aluminum (99.999%) mixed in stoichiometric ratios by arc-melting in a pure argon atmosphere. In order to ensure homogenization, the alloys were overturned and melted several times. The ingot of $CePt_2Al_2$ was divided into six parts, sealed in evacuated quartz ampoules, and annealed at 250 °C, 320 °C, 550 °C, 650 °C, 700 °C, and 800 °C for 720 h. Afterward, the ampoules were rapidly quenched to room temperature using cold water. The alloy of $CePt_3Al_3$ was annealed in an evacuated ampoule at 700 °C for 720 h.

2.2. Energy Dispersive X-Ray Analysis

Energy dispersive X-ray (EDX) analysis of all annealed samples was performed using a Carl Zeiss LEO EVO 50XVP scanning electron microscope (SEM) with an EDX-spectrometer INCA Energy 450 (Oxford Instruments). The accelerating voltage was 20 kV. For quantitative microanalysis, the INCA energy dispersion microanalysis system contains predefined standards for all elements. Analysis accuracy can be improved by incorporating proprietary measured reference materials. CePtAl was used as an external standard. The samples under investigation were placed together with the standard in a hot pressing machine (Bühler), filled with an electrically conductive resin, and formed into a tablet. The surface of the tablet was sanded using sandpaper cloths of different grain sizes and then polished

on a cloth with an Al_2O_3 paste. Finally, the tablet was washed for 5 min in an ultrasonic bath filled with ethanol. The uncertainty of measurements for each element did not exceed 0.7 at.%.

2.3. Powder X-Ray Diffraction

Powder X-ray diffraction (XRD) patterns for phase analysis and preliminary determination of unit cell parameters were obtained with a STOE STADI P transmission diffractometer ($CuK_{\alpha 1}$-radiation (λ = 1.54056 Å), Ge(111)-monochromator, a linear position-sensitive detector, 3–5° ≤ 2θ ≤ 93–95°, step scan 0.01°, 10 s counting time per point), using a WinXpow program [26].

2.4. High Temperature Powder Synchrotron X-Ray Diffraction

A high-intensity, high-resolution X-ray source (λ = 0.399962(13) Å) at the European Synchrotron Radiation Facility (ESRF, Grenoble, France) was used in the temperature-dependent powder XRD experiments.

The powder of the sample was placed in an evacuated thin-walled quartz glass capillary with a diameter of 0.5 mm, which was rotated during measurements at a rate of 1200 rpm to improve the counting statistics. Calibration of the goniometer and refinement of the X-ray wavelength were performed using the Si NIST 640c silicon standard. Synchrotron XRD patterns were measured at an angle range of 2° ≤ 2θ ≤ 22.912° with a scan step of 0.002°.

2.5. Crystal Structure Determination

The crystal structures of the tetragonal and orthorhombic modifications of $CePt_2Al_2$ as well as $CePt_3Al_3$ were determined from experimental powder XRD data. Indexing of the powder XRD pattern was performed using TREOR and DICVOL programs implemented in WinXpow [26] and FULLPROFF [27,28] packages.

Tetragonal $CePt_2Al_2$. The preliminary parameters of tetragonal $CePt_2Al_2$ were established using a low-quality single crystal found as a single copy in a sample of stoichiometric composition heated to 1200 °C and quenched in ice-cold water, which allowed us to attribute the structure to the $CaBe_2Ge_2$ type.

The tetragonal unit cell parameters obtained from powder XRD (Table 1) were compatible with the structure types of $ThCr_2Si_2$ and $CaBe_2Ge_2$. Analysis of the systematic reflection conditions indicated a primitive unit cell, therefore the $CaBe_2Ge_2$ type was chosen as a structural model. For the Rietveld refinement of tetragonal $CePt_2Al_2$ with the MRIA program [29], a high-temperature powder XRD pattern collected at 350 °C was used. In the refinement, the observed anisotropic line broadening was approximated in the quartic form [30] with five variables in the case of tetragonal syngony. The result of the refinement is shown in Figure 1a and Table 1.

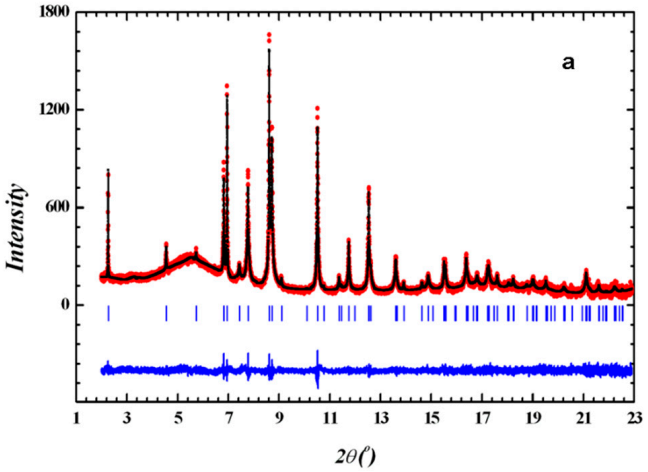

Figure 1. *Cont.*

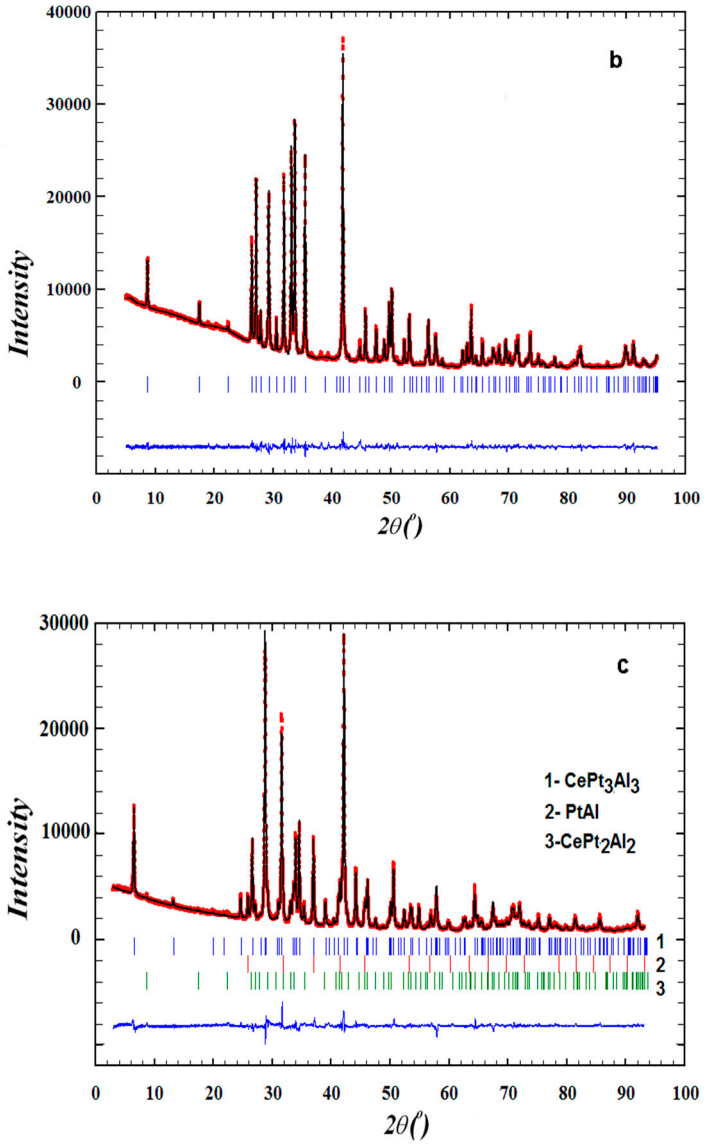

Figure 1. Observed (red dots), calculated (black solid line), and difference (bottom blue line) powder X-ray diffraction (XRD) patterns for tetragonal $CePt_2Al_2$ (**a**), orthorhombic $CePt_2Al_2$ (**b**), and $CePt_3Al_3$ (**c**).

Orthorhombic $CePt_2Al_2$ and $CePt_3Al_3$. Careful examination of the systematic extinctions in the orthorhombic $CePt_2Al_2$ and $CePt_3Al_3$ datasets suggested a *C*-centered unit cell ($h + k = 2n$ for all *hkl*), which prompted space groups *Cmme*, *Cm*2*e*, *C*2*me*, *Cmm*2, and *C*222. The best refinement results were obtained in the centrosymmetric space group *Cmme*. The structures of orthorhombic $CePt_2Al_2$ and $CePt_3Al_3$ were solved using the Patterson method with the SHELXS [31] program and sets of 115 and 162 reflection intensities, respectively, extracted from the powder XRD patterns after pseudo-Voigt fitting. The structures were refined via the Rietveld method using the FULLPROF program [27,28] for a single phase in the case of $CePt_2Al_2$ and for three phases in the case of $CePt_3Al_3$. For the latter, small impurities that had previously been detected by EDX (PtAl binary and orthorhombic $CePt_2Al_2$) were taken into account. The relevant crystallographic details for data collection and refinement are listed in Table 1; observed, calculated, and difference room-temperature XRD powder patterns are plotted in Figure 1b,c. The atomic coordinates and isotropic displacement parameters determined for tetragonal $CePt_2Al_2$, orthorhombic $CePt_2Al_2$, and $CePt_3Al_3$ are listed in Table 2, and selected interatomic distances are given in Table 3.

Table 1. Crystal data and structural refinement for the *ht*-$CePt_2Al_2$, *lt*-$CePt_2Al_2$, and $CePt_3Al_3$ compounds.

Empirical Formula	***ht*-$CePt_2Al_2$**	***lt*-$CePt_2Al_2$**	**$CePt_3Al_3$ ***
Molar mass, g/mol	584.26	584.26	806.33
Structure type, Pearson symbol	$CaBe_2Ge_2$, *tP*10	$CePt_2Al_2$, *oC*20	$CePt_3Al_3$, *oC*28
Space group, Z	*P*4/*nmm* (129), 2	*Cmme* (67), 4	*Cmme* (67), 4
Unit cell dimensions			
a, Å	4.3637(9)	5.84138(2)	6.36548(6)
b, Å	4.3637(9)	6.39099 (3),	5.78301(6)
c, Å	10.0925(14)	10.11611(5)	13.36245(19)
V, $Å^3$	192.18(6)	377.657	491.894(10)
Calculated density, g/cm^3	10.097	(3)10.276	10.888
T, K	623(1)	295(1)	298(2)
Radiation, λ, Å	synchrotron, 0.399962(13)	$CuK\alpha_1$, 1.54056	$CuK\alpha_1$, 1.54056
2θ range, step°	2–22.912, 0.002	5–95.19, 0.01	3–93.09, 0.01
Total no. reflections	79	115	162
Refined parameters no.	35	12	29
Rietveld reliability factors			
R_p	0.060	0.024	0.037
R_{wp}	0.069	0.035	0.050
R_{exp}	0.060	0.016	0.020
χ^2	1.334	5.54	5.99

* All indicators—R-factors, no. of parameters, etc. are given for the three-phases refinement.

Table 2. Atomic coordinates and isotropic displacement parameters in the crystal structures of *ht*-$CePt_2Al_2$, *lt*-$CePt_2Al_2$, and $CePt_3Al_3$.

Atom	Multiplicity, Wyckoff Letter, Site Symmetry	*x/a*	*y/b*	*z/c*	Uiso., $Å^2$
ht-$CePt_2Al_2$					
Ce1	2*c*(4*mm*)	1/4	1/4	0.7456(3)	0.0211(9)
Pt1	2*b*(-4*m*2)	3/4	1/4	1/2	0.0211(9)
Pt2	2*c*(4*mm*)	1/4	1/4	0.1316(3)	0.0211(9)
Al1	2*a*(-4*m*2)	3/4	1/4	0	0.0211(9)
Al2	2*c*(4*mm*)	1/4	1/4	0.3963(17)	0.0211(9)
lt-$CePt_2Al_2$					
Ce1	4*g*(*mm*2)	0	1/4	0.24780(15)	0.0117(4)
Pt1	4*a*(222)	1/4	1/2	0	0.0224(4)
Pt2	4*g*(*mm*2)	0	1/4	0.62972(11)	0.0146(3)
Al1	4*b*(222)	1/4	1/2	1/2	0.019(2)
Al2	4*g*(*mm*2)	0	1/4	0.8940(7)	0.013(2)
$CePt_3Al_3$					
Ce1	4*g*(*mm*2)	0	1/4	0.30545(16)	0.0097(7)
Pt1	8*l*(. . . 2)	1/4	1/2	0.11280(8)	0.0046(4)
Pt2	4*g*(*mm*2)	0	1/4	0.59815(12)	0.0064(5)
Al1	4*b*(222)	1/4	1/2	1/2	0.001(3)
Al2	4*g*(*mm*2)	0	1/4	0.7760(8)	0.039(5)
Al3	4*g*(*mm*2)	0	1/4	−0.0019(9)	0.057(5)

Table 3. Selected interatomic distances (d) in *ht*-$CePt_2Al_2$, *lt*-$CePt_2Al_2$, and $CePt_3Al_3$ structures.

***ht*-$CePt_2Al_2$**			***lt*-$CePt_2Al_2$**			**$CePt_3Al_3$**		
Atom 1	**Atom 2**	**d, Å**	**Atom 1**	**Atom 2**	**d, Å**	**Atom 1**	**Atom 2**	**d, Å**
Ce1	4Pt1	3.302(3)	Ce1	4Pt1	3.3120(11)	Ce1	4Pt1	3.3540(18)
	4Pt2	3.3251(18)		2Pt2	3.1727(7)		2Pt2	3.1655(11)
	4Al1	3.369(3)		2Pt2	3.4273(7)		2Pt2	3.4335(10)
	4Al2	3.402(7)		4Al1	3.3458(12)		4Al1	3.3736(16)
				2Al2	3.254(3)		2Al2	3.090(4)
				2Al2	3.503(3)		2Al2	3.364(4)
Pt1	4Al2	2.420(7)	Pt1	4Al2	2.416(3)	Pt1	2Al3	2.611(7)
	4Pt1	3.0856(6)		2Pt1	2.9207(10)		2Al2	2.614(6)
	4Ce1	3.302(3)		2Pt1	3.1955(15)		2Al3	2.640(7)
				4Ce	3.3120(11)		2Pt1	2.8915(13)
							Pt1	3.0146(15)
							2Pt1	3.1827(13)
							2Ce1	3.3540(18)
Pt2	4Al1	2.5544(15)	Pt2	4Al1	2.5313(6)	Pt2	Al2	2.377(11)
	Al2	2.672(17)		Al2	2.673(7)		4Al1	2.5185(8)
	4Ce1	3.3251(18)		2Ce1	3.1727(7)		2Ce1	3.1655(11)
				2Ce1	3.4273(7)		2Ce1	3.4335(10)
Al1	4Pt2	2.5544(15)	Al1	4Pt2	2.5313(6)	Al1	4Pt2	2.5185(8)
	4Al1	3.0856(6)		2Al1	2.9207(10)		2Al1	2.8915(13)
	4Ce1	3.369(3)		2Al1	3.1955(15)		2Al1	3.1827(13)
				4Ce1	3.3458(12)		4Ce	3.3736(16)
Al2	4Pt1	2.420(7)	Al2	4Pt1	2.416(3)	Al2	Pt2	2.377(11)
	Pt2	2.672(17)		Pt2	2.673(7)		4Pt1	2.614(6)
	4Ce1	3.402(7)		2Ce1	3.254(3)		Al3	2.968(16)
				2Ce1	3.503(3)		2Ce1	3.090(4)
							2Ce1	3.364(4)
						Al3	4Pt1	2.611(7)
							4Pt1	2.640(7)
							2Al3	2.8920(3)
							Al2	2.968(16)
							2Al3	3.1831(3)

Further details regarding the investigation of the crystal structures may be obtained from CCDC/FIZ: CSD-1988138 (tetragonal $CePt_2Al_2$), CSD-1988139 (orthorhombic $CePt_2Al_2$), and CSD-1988140 ($CePt_3Al_3$).

2.6. Differential Thermal Analysis

Thermal stability and temperature at which the structural phase transition of $CePt_2Al_2$ occurs were investigated by differential thermal analysis (DTA) at temperatures between 22 °C and 1200 °C, with a heating rate of 20° per minute in a stream of pure helium (sample mass ~20 mg) using a Netzsch STA449 F1 apparatus equipped with a Platinum RT analyzer.

3. Results and Discussion

3.1. Sample Characterization

Six samples of $Ce_{20.0}Pt_{40.0}Al_{40.0}$ (at.%) annealed at 250 °C, 320 °C, 550 °C, 650 °C, 700 °C, and 800 °C for 720 h were investigated by powder XRD and EDX analyses. For all samples, the main phase had the $Ce_{20.7}Pt_{39.9}Al_{39.4}$ (at.%) composition. The microstructure of the studied samples showed that the sample annealed at 800 °C was single-phase (Figure 2a), while those annealed at 250 °C, 320 °C, 550 °C, 650 °C, and 700 °C contained an additional unknown phase with a composition close to $Ce_{23.9}Pt_{50.7}Al_{25.4}$ (at.%).

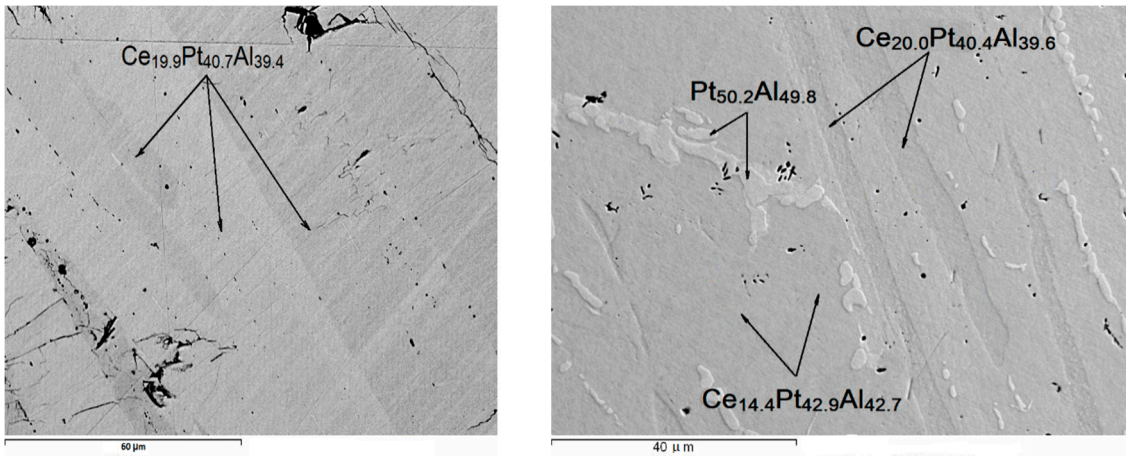

(**a**) (**b**)

Figure 2. Microstructure of the $Ce_{20.0}Pt_{40.0}Al_{40.0}$ (at.%) alloy annealed at 800 °C (**a**) and of the $Ce_{14.2}Pt_{42.9}Al_{42.9}$ (at.%) alloy annealed at 700 °C (**b**) obtained using scanning electron microscopy (SEM).

Microstructures of all samples are shown in Figure S1 in the Supplementary Materials. Microstructure of the $Ce_{14.2}Pt_{42.9}Al_{42.9}$ (at.%) alloy annealed at 700 °C showed that, in addition, to the main $Ce_{14.4}Pt_{42.9}Al_{42.7}$ (at.%) phase, the sample contained $Pt_{50.2}Al_{49.8}$ (at.%) and $Ce_{20.0}Pt_{40.4}Al_{39.6}$ (at.%) as admixtures (Figure 2b).

According to powder XRD patterns, all samples of $CePt_2Al_2$ including the as-cast one, were single-phase and solely contained an orthorhombic modification of $CePt_2Al_2$ (Figure 1b, Figure S2a–g). As follows from the XRD pattern of $CePt_3Al_3$ after annealing, the sample contained PtAl and $CePt_2Al_2$ admixtures in the amount of 4 mass % and 9 mass %, respectively (Figure 1c).

3.2. Thermal Analysis and Temperature-Dependent XRD

Since two crystallographic modifications were identified for the $CePt_2Al_2$ compound, tetragonal and orthorhombic, additional studies of the phase transition of $CePt_2Al_2$ were conducted. DTA (22–1200 °C) was performed for a sample annealed at 550 °C. The heating curve showed a weak endothermic effect at 280(1) °C, which could be attributed to a structural transition from a low-temperature polymorph to a high-temperature one (Figure S3). The endothermal effect at 1100 °C corresponded to the melting point. Attempts to obtain a high-temperature polymorph of $CePt_2Al_2$ by thermal quenching in cold water failed.

To study the stability of the crystallographic phases of $CePt_2Al_2$ and their structural transformation, in situ temperature-dependent synchrotron X-ray diffraction measurements were performed. Figure 3a,b clearly demonstrates the changes in X-ray patterns that occurred between 250 and 300 °C.

XRD patterns observed within the range of 25–250 °C corresponded to the low-temperature orthorhombic modification, *lt*-$CePt_2Al_2$. However, a change was detected at 300 and 350 °C that indicates a transition to a tetragonal modification, *ht*-$CePt_2Al_2$. The second series of in situ X-ray experiments with the same sample within a temperature range of 220–320 °C with 10° incremental increases in temperature (Figure S4a,b) demonstrated a transition at 280 °C. These data strongly support the results observed with DTA measurements and together clearly demonstrate the temperature at which structural phase transition occurs, providing proof of its reversible nature. Further analyses of powder XRD patterns collected at 300 and 350 °C yielded the crystal structure of *ht*-$CePt_2Al_2$ (Figure 1a).

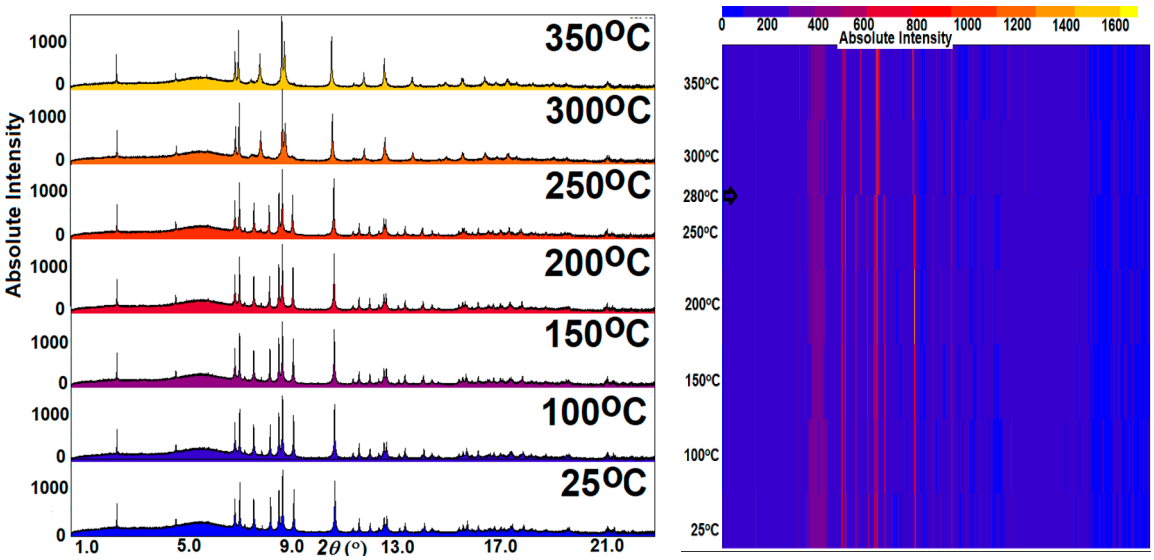

(**a**) (**b**)

Figure 3. Structural transition of the low-temperature orthorhombic $CePt_2Al_2$ to the high-temperature tetragonal modification. (**a**) XRD patterns measured at 25, 100, 150, 200, 250, 300, and 350 °C; (**b**) a projection of XRD patterns.

3.3. *$CePt_2Al_2$ Crystal Structures*

High-temperature modification of $CePt_2Al_2$ is a new representative of tetragonal $CaBe_2Ge_2$ type (space group *P*4/*nmm*, Pearson symbol *tP*10) with lattice parameters: a = 4.3637(9) Å, c = 10.0925(14) Å, and Z = 2 (Figure 1a). The *lt*-$CePt_2Al_2$ compound crystallizes with its own structure type (space group *Cmme*, Z = 4): a = 5.84138(2) Å, b = 6.39099(3) Å, c = 10.11611(5) Å (Figure 1b).

Though the general motif of the atomic arrangement in two polymorphs of $CePt_2Al_2$ seems very similar, some structure peculiarities can be pointed out.

***ht*-$CePt_2Al_2$**. Following the $CaBe_2Ge_2$ type, *ht*-$CePt_2Al_2$ is constructed from two types of corrugated $[Pt_2Al_2]$ layers perpendicular to [001], with cerium atoms situated between them (Figure 4a,b). In the Pt-based layer, interatomic distances Pt1–Al2 are equal to 2.420(7) Å, and in the Al-based layer, interatomic distances Pt2–Al1 are equal to 2.5544(15) Å, indicating significant chemical bonding in the layers. Neighboring $[Pt_2Al_2]$ layers of two types are connected by Pt2–Al2 contacts that are slightly longer (2.672(17) Å).

***lt*-$CePt_2Al_2$**. The orthorhombic modification *lt*-$CePt_2Al_2$ is a distorted variant of the high-temperature modification (Figure 4c,d). Symmetry reduction from tetragonal to orthorhombic involves differentiation of the lattice parameters a_{lt} and b_{lt}, which comprise diagonals $\boldsymbol{a + b}$ of the tetragonal unit cell of *ht*-$CePt_2Al_2$. Parameters a_{lt} and b_{lt} are related to those of the high-temperature polymorph as $a_{lt} \approx \sqrt{2}\, a_{ht}$ and $b_{lt} \approx \sqrt{2}\, a_{ht}$ with $a_{lt} < b_{lt}$. Parameter c remains relatively unchanged. The volume of the *lt*-$CePt_2Al_2$ unit cell is twice that of the *ht*-$CePt_2Al_2$ unit cell. The interatomic distances are similar to those observed in *ht*-$CePt_2Al_2$: Pt1–Al2 of 2.416(3) Å and Pt2–Al1 of 2.5313(6) Å within the layers, and Pt2–Al2 of 2.673(3) Å between the layers.

The Ce-centered polyhedra in both polymorphs can be described as hexagonal prisms of eight Pt and eight Al atoms with four additional atoms capping the side faces of the prisms. The range of Ce–Al and Ce–Pt bonding contacts are bigger in the structure of *lt*-$CePt_2Al_2$ compared to those in the *ht*-$CePt_2Al_2$ at 3.1727(7)–3.503(3) Å and 3.302(3)–3.402(7) Å, respectively. The platinum centered polyhedra can be regarded as a slightly distorted cuboctahedra (Pt1) and tetragonal antiprisms with one additional atom (Pt2). Aluminum atoms are located inside the distorted cuboctahedra (Al1) and mono-caped tetragonal antiprisms (Al2) (Table 3).

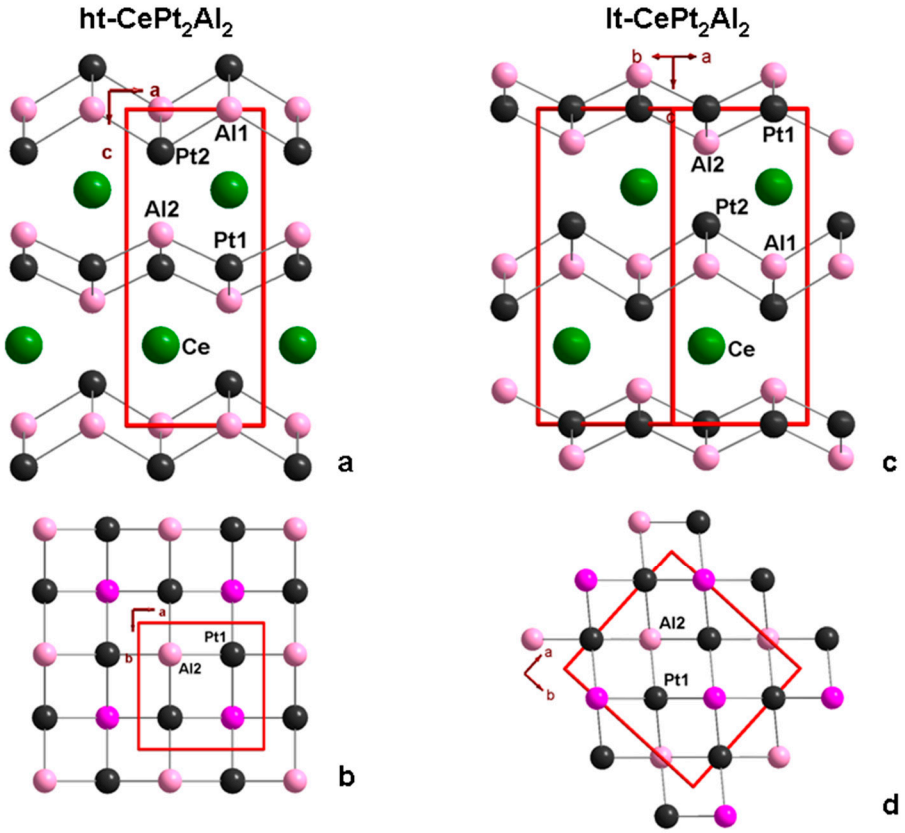

Figure 4. Crystal structures of two $CePt_2Al_2$ modifications: projection of *ht*-$CePt_2Al_2$ along the *b*-axis (**a**), projection of *lt*-$CePt_2Al_2$ in [110] (**c**), projections along the *c*-axis of the Pt-based layer of *ht*-$CePt_2Al_2$ (**b**), and of *lt*-$CePt_2Al_2$ (**d**). The Al2 atoms positioned above two-dimensional Pt-based basal layer are pink and those positioned below are rose. Unit cells are outlined in red.

3.4. $CePt_2Al_2$ Phase Transition

The observed phase transition can be attributed to a second-order transition. The space group of *lt*-$CePt_2Al_2$ (*Cmme)* is a subgroup of *ht*-$CePt_2Al_2$ (*P4/nmm)*. The main relationship in Bärnighausen formalism [32,33] is presented in Figure 5.

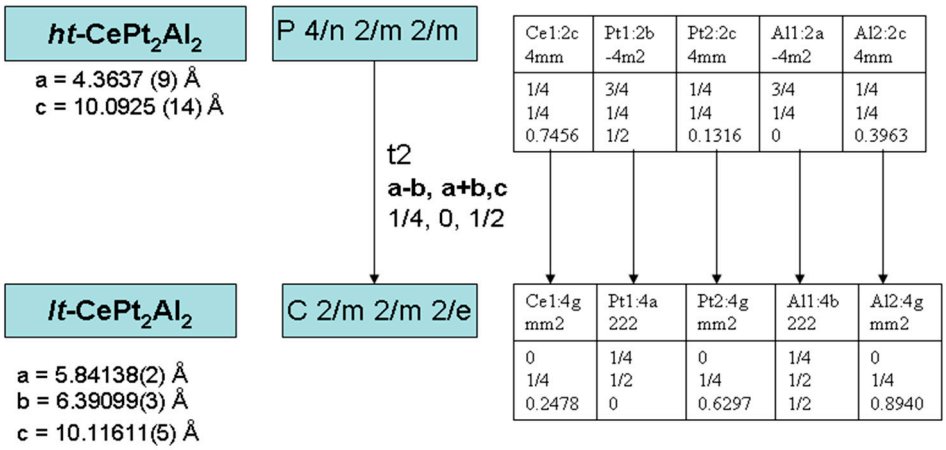

Figure 5. Group–subgroup scheme in the Bärnighausen formalism for the structures of *ht*-$CePt_2Al_2$ and *lt*-$CePt_2Al_2$.

The phase transition is of a displacive nature. Both modifications have a common structural motif and the same local atomic environment. On heating *lt*-$CePt_2Al_2$, Pt and Al atoms slightly shift in the directions indicated by the arrows in Figure 6, which leads to the equalization of the Pt1–Pt1, Al1–Al1, Ce–Pt2, and Ce–Al2 interatomic distances and of parameters *a* and *b*, and consequently, to transition from an orthorhombic to a tetragonal unit cell (Figure 7a, Table 3). There is no appreciable volume reduction in phase transformation. The formula unit volume increases continuously when heating from 25 °C to 350 °C with a negligible jump at the transition temperature (Figure 7b).

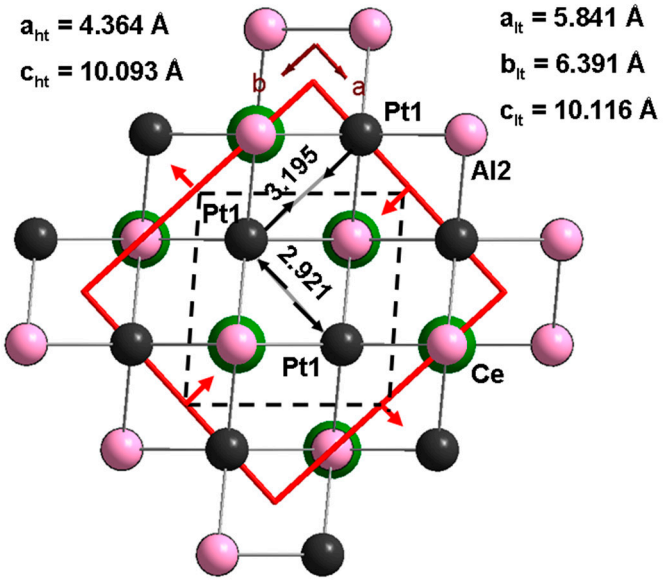

Figure 6. Projection of the crystal structure of *lt*-$CePt_2Al_2$ onto the (001) plane. The arrows indicate the direction of atomic displacements that lead to the transition to the tetragonal *ht*-$CePt_2Al_2$ modification. The orthorhombic unit cell is outlined in red, and the tetragonal cell with a black dashed line.

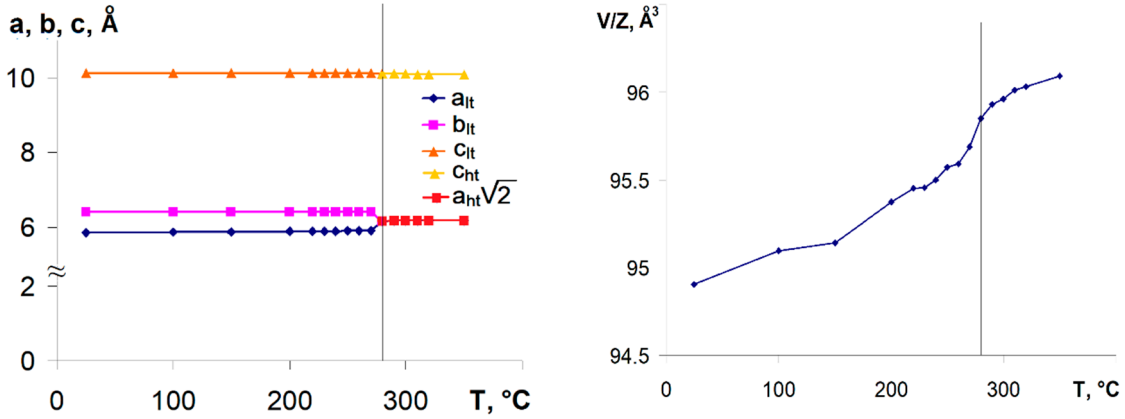

(**a**) (**b**)

Figure 7. Temperature-dependent evolution of the unit cell dimensions in $CePt_2Al_2$ (**a**) and of the scaled unit cell volume V/Z (Z is the formula unit per unit cell) (**b**). The error bars are smaller than the size of the plotted symbols and range from 0.0002 to 0.003 Å for parameters and from 0.3 to 0.6 Å^3 for scaled unit cell volumes.

A similar structural phase transition from the orthorhombic modification (*Cmme*) to the tetragonal modification (*P*4/*nmm*) for compounds with palladium—$LaPd_2Al_2$ and $CePd_2Al_2$—occurs at 91.5 (5) K and 13.5 (1) K, respectively [22]. Based on a comparison of cell dimensions, one can extrapolate that *lt*-$CePt_2Al_2$ is iso-structural with *lt*-$CePd_2Al_2$. The crystal structure of the latter compound was

not determined. The difference between a_{orth} and b_{orth} for *lt*-$CePt_2Al_2$ is equal to 0.55 Å, which is appreciably larger when compared to those for *lt*-$LaPd_2Al_2$ and *lt*-$CePd_2Al_2$ (0.12 Å and 0.14 Å, respectively).

3.5. $CePt_3Al_3$ Crystal Structure

The structure of $CePt_3Al_3$ reflects a distorted variant of the iso-stoichiometric $CePd_3Al_3$ compound [23] and crystallizes with its own type in the orthorhombic cell with dimensions a = 6.36548(6) Å, b = 5.78301(6) Å, c = 13.36245(19) Å, sp. gr. *Cmme*, Z = 4 (Figure 8a,b). Cell metrics of the $CePt_3Al_3$ and $CePd_3Al_3$ compounds correlate as follows: $a(CePt_3Al_3) \approx \sqrt{2}\, a(CePd_3Al_3)$, $b(CePt_3Al_3) \approx \sqrt{2}\, a(CePd_3Al_3)$, $c(CePt_3Al_3) \approx c(CePd_3Al_3)$, similar to the relationship between the metrics of *lt*-$CePt_2Al_2$ and *ht*-$CePt_2Al_2$. The group–subgroup relationship in Bärnighausen formalism [32,33] for the structures $CePt_3Al_3$ and $CePd_3Al_3$ is presented in Figure 8c. DTA of the $CePt_3Al_3$ sample did not demonstrate a thermal effect that indicated a possible phase transition.

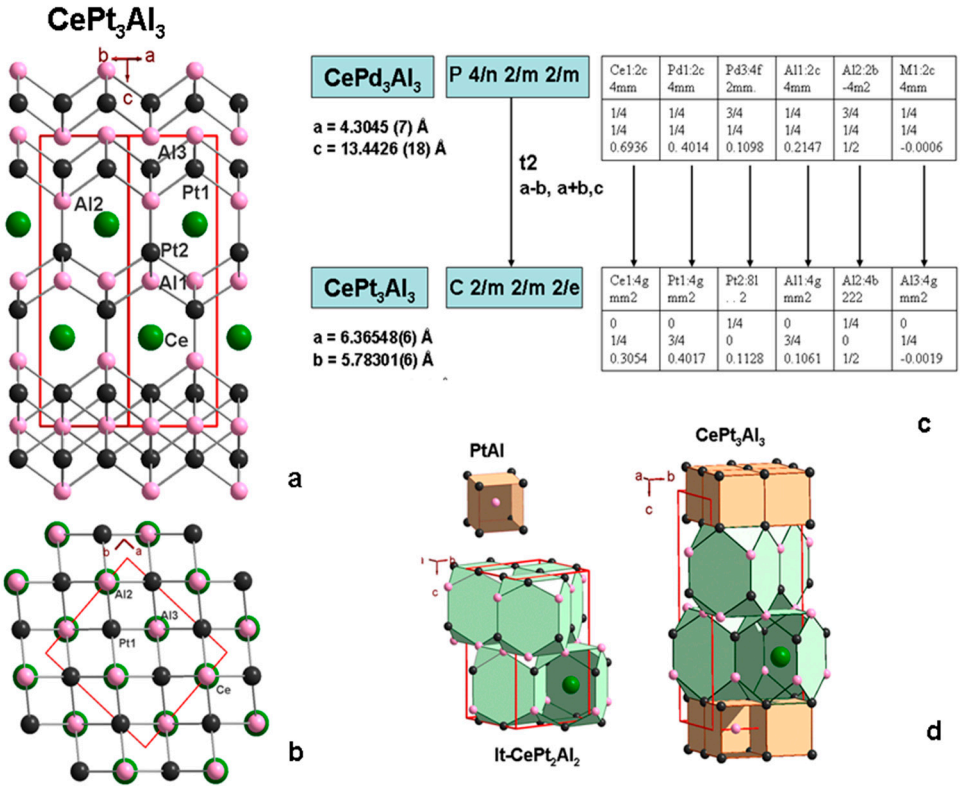

Figure 8. Crystal structure of $CePt_3Al_3$, with projection in [110] (**a**) and projection along the c-axis (**b**). Unit cells are outlined in red. Group–subgroup relations in the structures of $CePt_3Al_3$ and $CePd_3Al_3$ (**c**). Homologous series of $CePt_nAl_n$ (n = 2, 3) (**d**).

Similar to *lt*-$CePt_2Al_2$, $CePt_3Al_3$ contains two types of two-dimensional $[Pt_2Al_2]$ layers separated by Ce atoms. If the Al-based layer wholly complies with that of *lt*-$CePt_2Al_2$, two Pt-based layers are condensed to form a double layer in which capping Al atoms form the distorted squares of a planar network between two of those of Pt. The shortest Pt–Al interlayer distance Pt2–Al2 of 2.377(11) Å is significantly smaller than that of *lt*-$CePt_2Al_2$ and *ht*-$CePt_2Al_2$ (2.673 Å) and other Pt–Al contacts of $CePt_3Al_3$ of 2.5185(8)–2.640(7) Å (Table 3). A similarly short Pt–Al contact of 2.418(6) Å occurs in the $Ce_3Pt_4Al_6$ structure [34].

In $CePt_3Al_3$, coordination polyhedra of Ce, Pt, and Al atoms largely resemble those observed in *lt*-$CePt_2Al_2$ and *ht*-$CePt_2Al_2$. In the environment of the Al2 atom, an additional Al3 neighbor of the double layer results in the formation of a double-capped tetragonal antiprism around the Al2

atom. The Al3 atom is surrounded by eight platinum atoms with Pt–Al separations ranging within 2.611(7)–2.640(7) Å in the form of a distorted CsCl-like cube. With the next-nearest five neighbors at distances up to 3.1831(3) Å away, a polyhedron derived from the cuboctahedron is formed.

3.6. New Homologous Series

The structures of *lt*-$CePt_2Al_2$ and $CePt_3Al_3$ can be presented as Ce-centered polyhedra, sharing common edges in the *c*-direction and common hexagonal faces perpendicular to the *c*-axis (Figure 8d). Alternating along the *c*-axis, similar adjacent layers are inverted and shifted relative to each other. In the $CePt_3Al_3$ structure, the double layer of Ce-polyhedra alternate with the [PtAl] layer of CsCl-like distorted cubes (Figure 8d). Ternary compounds of *lt*-$CePt_2Al_2$ and $CePt_3Al_3$ comprise a new homologous series built of structural units of *lt*-$CePt_2Al_2$ and CsCl-type: $CePt_nAl_n$ (n = 2, 3). Due to the addition of one [PtAl] layer with a thickness of 3.138 Å to the *lt*-$CePt_2Al_2$ structure, the *c* parameter of the unit cell expands from 10.11611(5) Å in *lt*-$CePt_2Al_2$ to 13.36245(19) Å in $CePt_3Al_3$. Homologous series of iso-stoichiometric palladium compounds [23] contains one more member (n = 4), which is composed of alternating double Ce-polyhedra and double [PdAl] layers. An iso-stoichiometric compound with platinum was not observed.

3.7. Crystal Structures of Cerium Platinum Aluminides with High Al Content

The crystal structures analyzed consist of three-dimensional networks of Pt and Al forming Ce-centered hexagonal prisms of alternating Pt and Al atoms at the vertices, which were also observed in the structures of cerium platinum aluminides with high Al content: $CePtAl_3$ [35], $CePt_3Al_5$ [36], $Ce_4Pt_9Al_{13}$ [37], and $Ce_2Pt_9Al_{16}$ [38] (Figure 9). In these structures, one of the unit cell parameters is about 4.2 Å, which corresponds to the height of the Ce-hexagonal prism. In the structures of *ht*-$CePt_2Al_2$, *lt*-$CePt_2Al_2$, and $CePt_3Al_3$ as well as in $CePtAl_3$, there are two-dimensional layers of condensed Ce-centered hexagonal prisms, in contrast to the infinite isolated single channels of hexagonal prisms in $CePt_3Al_5$ and $Ce_2Pt_9Al_{16}$, and combinations of single and condensed triple channels of hexagonal prisms in the $Ce_4Pt_9Al_{13}$ compound (Figure 9).

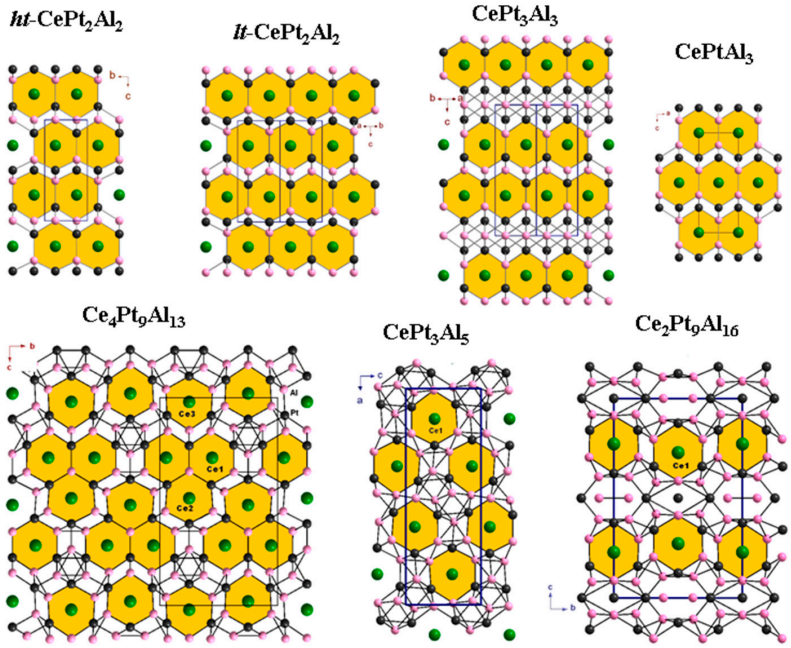

Figure 9. Projections of networks of crystal structures of *ht*-$CePt_2Al_2$, $CePtAl_3$, $Ce_4Pt_9Al_{13}$, $CePt_3Al_5$, and $Ce_2Pt_9Al_{16}$ in a direction along the smallest unit cell parameter and along [110] for *lt*-$CePt_2Al_2$ and $CePt_3Al_3$ structures. Ce, Pt, and Al atoms are drawn as green, black, and rose spheres, respectively. Single and triple Ce-atom channels and 2D Ce-atoms layers are highlighted in yellow.

4. Conclusions

Cerium platinum aluminides were synthesized. DTA and in situ temperature-dependent synchrotron X-ray diffraction measurements showed a reversible phase transition from a low-temperature orthorhombic $CePt_2Al_2$ of its own type to a high-temperature tetragonal $CePt_2Al_2$ of a $CaBe_2Ge_2$ type when heated to a temperature above 280 °C. The phase transition is of a displacive nature and associated with slight distortions of the $[Pt_2Al_2]$ layers. Orthorhombic compounds $CePt_2Al_2$ and $CePt_3Al_3$ present a new homologous series $CePt_nAl_n$ (n = 2, 3) formed from fragments of *lt*-$CePt_2Al_2$ and CsCl types.

Supplementary Materials: The following are available online at http://www.mdpi.com/2073-4352/10/6/465/s1, Figure S1: The microstructure of the $Ce_{20.0}Pt_{40.0}Al_{40.0}$ (at.%) samples annealed at 250 °C, 320 °C, 550 °C, 650 °C, and 700 °C; Figure S2(a–h): XRD patterns of $Ce_{20.0}Pt_{40.0}Al_{40.0}$ (at.%) samples; Figure S3: DTA heating thermogram of the $CePt_2Al_2$ sample; Figure S4: (a,b) Structural transition of low-temperature orthorhombic $CePt_2Al_2$ to a high-temperature tetragonal modification. XRD patterns at 220, 230, 240, 250, 260, 270, 280, 290, 300, 310, 320 °C (a); a projection of XRD patterns (b).

Author Contributions: Conceptualization, E.M. and Y.M.; Methodology, E.M. and A.T.; Formal analysis, Y.M. and Z.K.; Investigation, E.M., Y.M., Z.K., and A.T.; Resources, E.M.; Writing—original draft preparation, E.M.; Writing—review and editing, A.T.; Visualization, Y.M.; Supervision, E.M. and S.D.; Project administration, E.M.; Funding acquisition, E.M. All authors have read and agreed to the published version of the manuscript.

Funding: This study was supported by the Russian Foundation for Basic Researches (Grant No. 19-03-00135a).

Acknowledgments: The experimental data for the X-ray structure analysis were obtained using equipment at the Shared Physical Characterization Facilities Center, Kurnakov Institute of General and Inorganic Chemistry, Russian Academy of Sciences. The authors are indebted to ESRF-Grenoble for providing access to the ID22 Station (experiment MA-3313).

Conflicts of Interest: The authors have no conflicts of interest to declare. The funders had no role in the design of the study; in the collection, analyses, or interpretation of data; in manuscript composition, or in the decision to publish the results.

References

1. Dommann, A.; Hulliger, F.; Ott, H.R.; Gramlich, V. The crystal structure and some properties of $CePt_2Si_2$ and $CePt_2Ge_2$. *J. Less Common Met.* **1985**, *110*, 331–337. [CrossRef]
2. Beyermann, W.P.; Hundley, M.F.; Canfield, P.C.; Godart, C.; Selsane, M.; Fisk, Z.; Smith, J.L.; Thompson, J.D. Antiferromagnetism and enhanced specific heat in CeM_2Sn_2 (M = Ni, Ir, Cu, Rh, Pd and Pt). *Phys. B Condens. Matter* **1991**, *171*, 373–376. [CrossRef]
3. Zhang, P.; Zhai, H.F. Superconductivity in 122-type pnictides without iron. *Phys. B Condens. Matter* **2017**, *2*, 28. [CrossRef]
4. Imai, M.; Ibuka, S.; Kikugawa, N.; Terashima, T.; Uji, S.; Yajima, T.; Kageyama, H.; Hase, I. Superconductivity in 122-type antimonide $BaPt_2Sb_2$. *Phys. Rev. B* **2015**, *91*, 014513. [CrossRef]
5. Kitagawa, J.; Ishikawa, M. Magnetic properties and structural phase transition of $CePd_2Ga_2$ with $CaBe_2Ge_2$-type structure. *J. Phys. Soc. Jpn.* **1999**, *68*, 2380–2383. [CrossRef]
6. Takabatake, T.; Tanaka, T.; Bando, Y.; Fudjii, H.; Takeda, N.; Ishikawa, M.; Oguro, I. Magnetic and structural transitions in $CeRh_2Sb_2$. *Phys. B Condens. Matter* **1997**, *230–232*, 223–225. [CrossRef]
7. Doležal, P.; Klicpera, M.; Prchal, J.; Yavorský, P. Structural phase transition in $CePd_2Ga_2$ under hydrostatic pressure. *Acta Phys. Pol. A* **2015**, *127*, 219–221. [CrossRef]
8. Eisenmann, B.; May, N.; Müller, W.; Schäfer, H. Eine neue strukturelle Variante des $BaAl_4$-Typs: Der $CaBe_2Ge_2$-Typ. *Z. Nat. B* **1972**, *27*, 1155–1157. [CrossRef]
9. Ban, Z.; Sikirica, M. The crystal structure of ternary silicides ThM_2Si_2 (M = Cr, Mn, Fe, Co, Ni, Cu). *Acta Crystallogr.* **1965**, *18*, 594–599. [CrossRef]
10. Bruzzone, G.; Merlo, F. The strontium-aluminium and barium-aluminium systems. *J. Less Common Met.* **1975**, *39*, 1–6. [CrossRef]
11. Shelton, R.N.; Braun, H.F.; Musick, E. Superconductivity and relative phase stability in 1:2:2 ternary transition metal silicides and germanides. *Solid State Common* **1984**, *52*, 797–799. [CrossRef]

12. Hiebl, K.; Rogl, P. Magnetism and structural chemistry of ternary silicides: (RE, Th, U) Pt_2Si_2 (RE = Rare Earth). *J. Magn. Magn. Mater.* **1985**, *50*, 39–48. [CrossRef]
13. Rossi, D.; Marazza, R.; Ferro, R. Ternary RM_2X_2 alloys of the rare earths with the precious metals and silicon (or germanium). *J. Less Common Met.* **1979**, *66*, 17–25. [CrossRef]
14. Mayer, I.; Yetor, P.D. MPt_2Si_2 compounds of the $ThCr_2Si_2$ type. *J. Less Common Met.* **1977**, *55*, 171–176. [CrossRef]
15. Venturini, G.; Malaman, B.; Roques, B. A monoclinic variant of the tetragonal $CaBe_2Ge_2$-type structure. *J. Less Common Met.* **1989**, *146*, 271–278. [CrossRef]
16. Imre, A.; Hellmann, A.; Mewis, A. $LaPt_2Ge_2$ und $EuPt_2Ge_2$ – Neubestimmung der Kristallstrukturen. *Z. Anorg. Allg.Chem.* **2006**, *632*, 2217–2221. [CrossRef]
17. Selsane, M.; Lebail, M.; Hamdaoui, N.; Kappler, J.P.; Noel, H.; Achard, J.C.; Godart, C. Structural, magnetic and valence properties of CeM_2Sn_2 (M = Ni, Cu, Rh, Pd, Ir, Pt). *Phys. B Condens. Matter* **1990**, *163*, 213–215. [CrossRef]
18. Wenski, G.; Mewis, A. $BaAl_4$-Denvative Structures of ARu_2X_2 (A = Ca, Sr, Ba, Eu; X—P, As) and of APt_2P_2 (A = Ca, Eu). *Z. Nat. B* **1986**, *41b*, 38–43. [CrossRef]
19. Imre, A.; Hellmann, A.; Wenski, G.; Graf, J.; Johrendt, D.; Mewis, A. Inkommensurabel modulierte Kristallstrukturen und Phasenumwandlungen—Die Verbindungen $SrPt_2As_2$ und $EuPt_2As_2$. *Z. Anorg. Allg. Chem.* **2007**, *633*, 2037–2045. [CrossRef]
20. Hulliger, F.; Nissen, H.U.; Wessicken, R. On new $CaBe_2Ge_2$-type representatives MAu_2AI_2. *J. Alloys Compd.* **1994**, *206*, 263–266. [CrossRef]
21. Schank, C.; Jfihrling, F.; Luo, L.; Grauel, A.; Wassilew, C.; Borth, R.; Olesch, G.; Bredl, C.D.; Geibel, C.; Steglich, F. 4f-conduction electron hybridization in ternary Ce-TM-A1 compounds. *J. Alloys Compd.* **1994**, *207*, 329–332. [CrossRef]
22. Chapona, L.C.; Goremychkina, E.A.; Osborn, R.; Rainford, B.D.; Short, S. Magnetic and structural instabilities in $CePd_2Al_2$ and $LaPd_2Al_2$. *Phys. B Condens. Matter* **2006**, *378–380*, 819–820. [CrossRef]
23. Tursina, A.; Khamitcaeva, E.; Gribanov, A.; Gnida, D.; Kaczorowski, D. $CePd_2Al_2$, $CePd_3Al_3$, and $CePd_4Al_4$, A New Homologous Series Built of $CaBe_2Ge_2$- and CsCl-type Units. *Inorg. Chem.* **2015**, *54*, 3439–3445. [CrossRef] [PubMed]
24. Bukhanko, N.; Gribanov, A.; Kaldarar, H.; Royanian, E.; Michor, H.; Bauer, E.; Murashova, E.; Seropegin, Y.; Grytsiv, A.; Rogl, P.; et al. Novel $CePt_2Al_2$: Crystal structure and physical properties. In Proceedings of the 16th International Conference on Solid Compounds of Transition Elements, Dresden, Germany, 26–31 July 2008; p. 172.
25. Morozova, Y.S.; Tursina, A.I.; Dunaev, S.F.; Murashova, E.V. Ternary intermetallic compound $CePt_3Al_3$. In Proceedings of the VIIIth National Crystal Chemistry Conference, Suzdal, Russia, 30 May–3 June 2016; p. 181.
26. *STOE WinXPOW (Version 2.24)*; Stoe & Cie GmbH: Darmstadt, Germany, 1999.
27. Rodriguez-Carvajal, J. Recent Developments of the Program FULLPROF, in Commission on Powder Diffraction (IUCr). *Newsletter* **2001**, *26*, 12–19.
28. Roisnel, T.; Rodriguez-Carvajal, J. Materials science forum. In Proceedings of the European Powder Diffraction Conference, Warsaw, Poland, 19–22 September 2008; p. 118.
29. Zlokazov, V.B.; Chernyshev, V.V. MRIA—A program for a full profile analysis of powder multiphase neutron-diffraction time-of-flight (direct and Fourier) spectra. *J. Appl. Crystallogr.* **1992**, *25*, 447–451. [CrossRef]
30. Popa, N.C. The (*hkl*) dependence of diffraction line broadening caused by strain and size for all Laue groups in Rietveld refinement. *J. Appl. Crystallogr.* **1998**, *31*, 176–180. [CrossRef]
31. Sheldrick, G.M. Crystal structure refinement with SHELXL. *Acta Crystallogr. Sect. C Struct. Chem.* **2015**, *71*, 3–8. [CrossRef]
32. Bärnighausen, H. Group-subgroup relations between space groups: A useful tool in crystal chemistry. *MATCH Commun. Math. Chem.* **1980**, *9*, 139–175.
33. Müller, U. Kristallographische gruppe-untergruppe-beziehungen und ihre anwendung in der kristallchemie. *Z. Anorg. Allg. Chem.* **2004**, *630*, 1519. [CrossRef]
34. Tursina, A.I.; Gribanov, A.V.; Bukhan'ko, N.G.; Rogl, P.; Seropegin, Y.D. Crystal structure of the novel compound $Ce_3Pt_4Al_6$. *Chem. Met. Alloys* **2008**, *1*, 62–66. [CrossRef]

35. Mock, S.; Pfleiderer, C.; Lohneysen, H. Low-temperature properties of $CeTAl_3$ (T = Au, Cu, Pt) and $CeAuGa_3$. *J. Low Temp. Phys.* **1999**, *115*, 1–14. [CrossRef]
36. Tursina, A.I.; Bukhan'ko, N.G.; Gribanov, A.V.; Shchelkunov, V.A.; Nelyubina, Y.V. A new ternary aluminide, $CePt_3Al_5$. *Acta Crystallogr. Sect. E Struct. Rep. Online* **2005**, *61*, i285–i286. [CrossRef]
37. Morozova, Y.; Gribanov, A.; Murashova, E.; Dunaev, S.; Grytsiv, A.; Rogl, P.; Giester, G.; Kaczorowski, D. Novel ternary compound $Ce_4Pt_9Al_{13}$: Crystal structure, physical properties. *J. Alloys Compd.* **2018**, *767*, 496–503. [CrossRef]
38. Tursina, A.; Murashova, E.; Noël, H.; Bukhan'ko, N.; Seropegin, Y. Crystal structure and magnetic properties of the new intermetallic $Ce_2Pt_9Al_{16}$. *Intermetallics* **2009**, *17*, 780–783. [CrossRef]